






Magnetic barrier and electric field effects on exciton-polaron relaxation and transport properties in transition metal dichalcogenide monolayers

C. Kenfack-Sadem ^{1,2,*}, A. K. Tegoumouet ³, A. B. Moubissi ⁴, Natalia Cortés ⁵, M. F. C. Fobasso ¹,
M. Masale,⁶ and A. Kenfack-Jiotsa⁷

¹Laboratory of Condensed Matter and Nanomaterials, Department of Physics,
University of Dschang, P.O. Box 67, Dschang, Cameroon

²International Chair in Mathematical Physics and Applications (ICMPA-UNESCO Chair),
University of Abomey-Calavi, 072 P.O. Box 50, Cotonou, Republic of Benin

³Laboratoire de Mécanique-Matériaux et Structures, Département de Physique, Université de Yaoundé I, BP 812, Yaoundé, Cameroon

⁴Faculté des Sciences, Université des Sciences et Techniques de Masuku B.P. 901, Franceville, Gabon

⁵Instituto de Alta Investigación, Universidad de Tarapacá, Casilla 7D, Arica, Chile

⁶University of Botswana, P/Bag 0022, Gaborone, Botswana

⁷Département de Physique, Ecole Normale Supérieure, Université de Yaoundé I, BP 42, Yaoundé, Cameroon



(Received 31 May 2022; revised 9 September 2022; accepted 23 January 2023; published 14 February 2023)

The relaxation of excitonic polaron and the transport properties in two-dimensional monolayers of transition metal dichalcogenides (TMDCs) such as MoS₂, MoSe₂, WSe₂, and WS₂ are investigated under the influence of a magnetic barrier and an electric field using the relaxation-time approximation and the Kubo formula. We find that the presence of magnetic barrier strengthens the electron-hole interaction and stabilizes the exciton-polaron while the electric field alters this stability. In addition, exciton-polaron is more relaxed as the electric field increases but due to the magnetic barrier it quickly returns into its equilibrium. Moreover, the electrical conductivity of TMDCs is favored by the electric field and a barrier of high magnetic lengths. MoSe₂ is the compound that presents the highest relaxation time and electrical conductivity. The result indicates that the electrical conductivity grows when the system is relaxed. The thermoelectric power of TMDCs falls when the electric field increases, whereas it does not present a monotonic behavior in the magnetic barrier. It globally decreases for weak values of the magnetic length and enhances for high values. The highest thermoelectricity is obtained in MoSe₂. A high optical conductivity is observed in TMDCs. The result shows that optical transitions rise as the magnetic strength of the barrier increases, but the electric field presents an opposite effect. The probability of absorb energy $\hbar\omega$ by the exciton-polaron steps up when the magnetic length and electric field increase. The highest value of optical conductivity and oscillator strength is observed for MoS₂. We demonstrate that the magnetic barrier and electric field are suitable parameters which can be used to improve the performance of TMDCs materials.

DOI: [10.1103/PhysRevB.107.075134](https://doi.org/10.1103/PhysRevB.107.075134)

I. INTRODUCTION

Due to their structures and different applications, transition metal dichalcogenides (TMDCs) are suitable two-dimensional (2D) materials with formula MX_2 , where the transition metal atoms M are sandwiched between two layers of chalcogen atoms X , and the MX_2 layers are coupled to each other by van der Waals interactions. Their semiconductor characteristics presenting high stability and flexibility [1–3] makes them highly interesting in many areas [4–6]. Their optical and electronic properties [7,8] reveal applications in valleytronics and spintronics [9,10], as well as in photoluminescence experiments [11].

An exciton-polaron is a quasiparticle resulting from the interaction of exciton (pair of electron-hole) with phonons, which are present in TMDCs [12,13]. Some authors have developed excitonic polaron systems where diagonalization

techniques are needed for suitable energy spectra and properties in 2D materials [14–16]. Excitonic systems are limited by the process of dressing with phonons [17–19], which itself can be understood through the relaxation phenomenon. The relaxation time is a good concept to study these systems due to the fact that exciton generation and recombination, and optical excitation depend on it [20,21]. Experimentally, it is found that the relaxation-time range is around femtosecond (fs) and picosecond (ps) [22–24]. The relaxation and the exciton generation are studied in PbS quantum dots [25]. It is seen that the confinement has an important role in these processes [26], and also in optical conductivity [27]. The appearance of an excitonic signal in the optical conductivity response has been demonstrated in ZnO [28] and graphene [29], revealing that exciton effects play an important role in the optical spectra. In semiconductors GaAs [30,31], the excitonic signal is observed for energies below the gap, by a peak in the absorption spectra. Above the gap, a renormalization of the band and the increase of the optical conductivity occur due to the scattering between electrons and holes. In addition, Peres *et al.* [32]

*kevinsadem@yahoo.fr

proved that an excitonic resonance in graphene is responsible for the measured midinfrared response, the broadening of the absorption at the threshold, the increase of the conductivity beyond the universal value above the Fermi blocked regime, and the reduction of the conductivity at high frequencies.

Yang *et al.* [33] studied the layer dependence on electrical and optoelectronic properties in ReSe₂. It is shown that the number of layers considerably influences these properties. For example, the band gap increases when the number of layers decreases, and a single layer provides best performance for mobility. Chen *et al.* [34] demonstrated the increase of electrical conductivity with the decrease in thickness layer. This implies the probable surface dominance of electrical conduction in TMDC layers resulting from either the intrinsic high surface conductivity or the anisotropic conductivity. Qin *et al.* [35] studied the in-plane effect of electron (hole) concentration at 300 K on the transport coefficients. Anisotropic behavior is observed for the thermopower and electrical conductivity. The electrical conductivity enhances when the carrier concentration increases, whereas the Seebeck coefficient decreases. They found that the Seebeck coefficient presents a lower asymmetry for *n*-type doping than for *p*-type doping. High amplitudes for the Seebeck coefficient are seen and a peak is observed at a carrier concentration of $1.25 \times 10^{11} \text{cm}^{-2}$. In addition, recently Ge *et al.* [36] have combined first-principles calculations and Boltzmann theory to demonstrate the high performance for the carrier transport in TMDCs. High Seebeck coefficient at low temperature and low electrical conductivity at high temperature are observed. They showed that the carrier transport can be due to the modest carrier effective mass and the weak electron (hole)-phonon coupling. It is clear that these properties are crucial in the study of charge-carrier transport in TMDC materials. It is well known that the behavior of quasiparticles such as polaron and exciton is considerably influenced by its environment, which can be an external magnetic field [37,38] or an electric field [39,40].

It has been shown that the applying of magnetic field on TMDCs leads to the increase of exciton binding energy with the magnetic strength [41]. Nam *et al.* [42] proved that the role of external magnetic field is minor on the electrical conductivity for very strong magnetic strength, and it becomes relatively significant for temperatures less than 200 K. Das *et al.* [43] showed a reduction of the Seebeck coefficient with an applied magnetic field and it enhances globally when the chemical potential and temperature increase. Tahir *et al.* [44] showed that the magneto-optical transport properties in monolayer (1L) 2D phosphorene are very influenced by a magnetic field. It is found that the optical conductivity has an oscillatory dependence on the magnetic field and the strength of optical transitions is a function of the *xy*-plane momentum operator. The magneto-optical response in TMDCs can be tuned in the visible, in the range of microwave to terahertz, contrary to graphene or a 2D electron gas, which are limited to the terahertz range. Reference [45] revealed that the real part of the optical conductivity is an increasing function of the temperature for WTe₂. In TMDCs [46], the attractive branch of excitonic polaron is not influenced enough by the magnetic strength, while the repulsive ones exhibit magnetic peaks and oscillations reflecting combined exciton-cyclotron resonance.

In 2D materials, the anomalous transport of exciton in response to an in-plane electric field is studied [47]. It is shown that during a very short time, there is a regime in which the velocities of electron and hole (which constitute the exciton) are in the same direction. The electron and hole initially move in separate directions until reaching an equilibrium, in which the Coulomb interaction is closer to the force of the electric field. In addition, applying an electric field considerably increases the relaxation time [48] and reduces the optical absorption [49] in GaAs quantum wells. The exciton binding energy decreases with the increase of the electric field and quantum-dot radius [50].

In this paper, we theoretically investigate the transport properties in typical 1L TMDCs: MoSe₂, WS₂, WSe₂, and MoS₂. The paper organization is as follows: the second section is the model and calculations in which we derive the analytical expressions of the ground-state (GS) energy, the relaxation time, the electrical conductivity, the optical conductivity, the Seebeck coefficient, and the oscillator strength. In Sec. III, we present the results and discussion of the magnetic barrier and in-plane electric field effects on these properties, whereas the conclusion summarizes in the last section.

II. MODEL AND CALCULATIONS

The system is taken as an exciton under the influence of a magnetic barrier and an electric field, interacting with longitudinal optical (LO) phonons in a 1L TMDC. The total Hamiltonian is written as

$$\hat{H} = \hat{H}_{ex}^{2D} + \hat{H}_{ph} + \hat{H}_{ex-ph}^{2D}. \quad (1)$$

Here, \hat{H}_{ex}^{2D} represents the Hamiltonian of the exciton (electron-hole) [49,51] in the TMDC *xy* plane, including the magnetic barrier and the electric field as

$$\begin{aligned} \hat{H}_{ex}^{2D} = & \frac{(P_{e,x}^2 + P_{e,y}^2)}{2m_e} - eE_{el}y_e + \frac{(P_{h,x}^2 + P_{h,y}^2)}{2m_h} + eE_{el}y_h \\ & + \frac{e^2 A_y^2}{2\mu} - \frac{e^2}{\varepsilon|\rho_e - \rho_h|}. \end{aligned} \quad (2)$$

where $\vec{P}_h(\vec{P}_e)$ is the hole (electron)-momentum vector, $\rho_e(\rho_h)$ represents the electron (hole) coordinate in the TMDC *xy* plane, and E_{el} is the electric field along the *y* direction. $m_e(m_h)$ is the effective mass of electron (hole), μ is the effective reduced mass of the exciton $(1/\mu) = (1/m_e) + (1/m_h)$, $e(-e)$ is the hole (electron) charge, and ε is the TMDC permittivity.

The magnetic barrier is characterized by the magnetic strength [52] $\vec{B}(0, 0, B_z)$, with $B_z(x) = B_0 l_B [\delta(x) - \delta(x-L)]$. The width of the barrier is denoted by L taken at 150 nm, and l_B is the magnetic length related to a standard magnetic field given by $B_0 = \hbar/(el_B^2)$. From the Dirac delta function, the magnetic field can also take the form

$$B_z(x) = \begin{cases} B_0 l_B; & \text{if } x = 0 \\ -B_0 l_B; & \text{if } x = L \\ 0; & \text{otherwise} \end{cases}. \quad (3)$$

Such magnetic barrier can be constructed as shown by Ghosh *et al.* [53]. Figure 1 illustrates the present case where two long narrow magnetic stripes are placed perpendicular

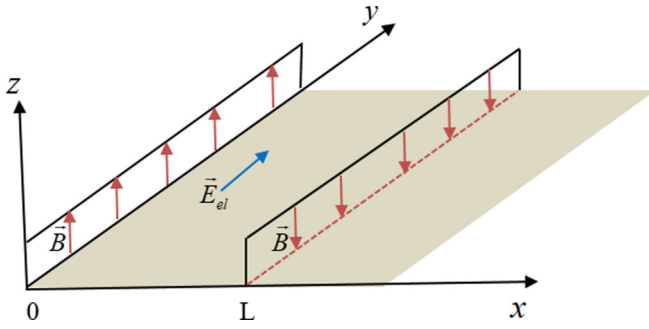


FIG. 1. Schematic of a TMDC system (light-brown 2D plane) under a magnetic barrier using two long narrow magnetic stripes with a magnetic field B (red arrows) along the z axis, and an electric field E_{el} along the y axis (blue arrow).

to the TMDC layer, respectively, at $x = 0$ (with $B_0 l_B$) and $x = L$ (with $-B_0 l_B$). The magnetic vector potential $\vec{A}(0, A_y, 0)$ is given by

$$A_y(x) = B_0 l_B [\Theta(x) - \Theta(x - L)] = \begin{cases} A; & 0 < x < L \\ 0; & \text{otherwise} \end{cases}, \quad (4)$$

where $A = \hbar/(el_B)$ and Θ is the Heaviside function.

The phonon's Hamiltonian appears as $\hat{H}_{ph} = \sum_q \hbar\omega_0 b_q^+ b_q$. $\hbar\omega_0$ denotes the phonon's energy while b_q and b_q^+ are, respectively, the annihilation and creation phonon operators, q is the phonon wave vector. The third term of Eq. (1) denotes the Hamiltonian of the exciton-phonon interaction taken as [54,55]

$$\hat{H}_{ex-ph}^{2D} = \sum_{K,q} \Xi^{op}(q) C_{K+q}^+ C_K (b_q + b_{-q}^+), \quad (5)$$

where C_K^+ (C_K) denotes the creation (annihilation) operator of an exciton, and K is the 2D wave vector of the exciton. The exciton-optical phonon-coupling function is given by

$$\Xi^{op}(q) = (D_c^{op} - D_v^{op}) \sqrt{\frac{\hbar q}{2S\eta u}}. \quad (6)$$

S represents the area of the TMDC layer, η denotes the area mass density, and u is the sound velocity. The deformation potential constant is D_v^{op} (D_c^{op}) for hole (electron)-LO phonon coupling at some critical points (K' , K) inside the valence (conduction) band.

In order to simplify the calculations, we can do a useful transformation for the exciton Hamiltonian term in Eq. (2) as

$$\hat{H}_{ex}^{2D} = \sum_K \lambda C_K^+ C_K. \quad (7)$$

We use the relative coordinate ($\vec{\rho} = \vec{\rho}_e - \vec{\rho}_h$), the center of mass ($\vec{R} = \frac{m_e}{M}\vec{\rho}_e + \frac{m_h}{M}\vec{\rho}_h$), and the 2D wave function $\Psi^{2D} = \exp(i\vec{K}^* \cdot \vec{R}) \sqrt{\frac{2}{\pi}} \frac{1}{a} \exp(-\frac{\rho}{a})$, with $\vec{K}^* = \vec{K} - \frac{e}{\hbar}\vec{A}$, a the exciton Bohr radius [51,56]. Then, the eigenenergy λ for the 2D exciton is obtained as

$$\lambda(K, l_B, E_{el}) = E_g + \frac{\hbar^2 K^2}{2M} - E_b + \xi_B - \xi_{el}. \quad (8)$$

The exciton energy is then quantified. E_g stands for the gap energy of the 1L MX_2 , the second term of Eq. (8) is the kinetic energy with the exciton effective mass $M = m_e + m_h$, E_b is the free-exciton binding energy, while ξ_{el} and ξ_B represent, respectively, the electric and magnetic parameters appearing as

$$\xi_B = \frac{\hbar^2}{l_B^2} \left(\frac{1}{2M} + \frac{1}{2\mu} \right); \quad \xi_{el} = 2eaE_{el}/\pi. \quad (9)$$

In the latest equation, the terms $\frac{\hbar^2}{2M}$ and $\frac{\hbar^2}{2\mu}$ refer, respectively, to the kinetic and binding energies. The magnetic barrier contributes both in the kinetic and binding energies of exciton, whereas the electric field which is directly linked to the charge (e) modifies the Coulomb interaction of the electron-hole pair. The barrier acts as an effective potential for the exciton motion and modifies the kinetic-energy operator. Moreover, the field is along the z direction confining the particles in the plane; then, electron and hole can acquire great kinetic energy.

We use an approximate method to diagonalize the full Hamiltonian (see Appendix A). The transformed Hamiltonian ($\hat{\Gamma}$) is averaged with the GS wave function $|\Psi_0\rangle = C_K^+ |0\rangle_k |0\rangle_{ph}$ to obtain the energy as

$$E_K = \left(\frac{\hbar^2 K^2}{2M} \right) (1 - G_{ex2}) - G_{ex1} + E_g - E_b + \xi_B - \xi_{el}. \quad (10)$$

One can see that the magnetic barrier and electric field modify the GS energy of excitonic polaron.

A. Relaxation time

The dynamic of polaronic systems is related to the fact that the time of optical phonons is approximately constant and finite. The presence of both electric and magnetic fields perturbs the excitonic states and the behavior of the system. The relaxation time (τ) of the exciton-polaron can take the form [37]

$$\frac{1}{\tau} = \frac{2\pi}{\hbar} \sum_q \{ |\Xi(q)|^2 \{ [n_B + f(E_{K+q})] \delta(E_K - E_{K+q} + \hbar\omega_0) + [1 + n_B - f(E_{K+q})] \delta(E_K - E_{K+q} - \hbar\omega_0) \}, \quad (11)$$

where n_B is the Bose-Einstein function and f is the Fermi-Dirac distribution with the Fermi energy (E_F),

$$n_B = [\exp(\beta E_K) - 1]^{-1} \\ f(E_{K+q}) = [1 + \exp(\beta(E_{K+q} - E_F))]^{-1}. \quad (12)$$

β denotes the inverse of the temperature. We develop the Dirac delta functions to obtain suitable forms for calculations (see Appendix B). Then, converting the summation of Eq. (11) into an integration, and integrating over q , one gets

$$\frac{1}{\tau} = \frac{M(D_c^{op} - D_v^{op})^2}{\pi \eta u (1 - G_{ex2}) \hbar^2} K \{ [n_B + f(E_K + \hbar\omega_0)] I_K^+ + [1 + n_B - f(E_K - \hbar\omega_0)] I_K^- \}, \quad (13)$$

where the integrals I_K^+ and I_K^- are given by

$$I_K^+ = \int_0^{2\pi} d\theta \frac{\cos^2\theta + \frac{M\hbar\omega_0}{\hbar^2 K^2(1-G_{ex2})}}{\sqrt{\cos^2\theta + \frac{2M\hbar\omega_0}{\hbar^2 K^2(1-G_{ex2})}}}, \quad (14)$$

$$I_K^- = \int_0^{2\pi} d\theta \frac{\cos^2\theta - \frac{M\hbar\omega_0}{\hbar^2 K^2(1-G_{ex2})}}{\sqrt{\cos^2\theta - \frac{2M\hbar\omega_0}{\hbar^2 K^2(1-G_{ex2})}}}. \quad (15)$$

These integrals are solved using the elliptic integrals of the first and second kind. This leads to

$$I_K^+ \approx \pi \left[\frac{\sqrt{\hbar^2 K^2(1-G_{ex2}) + 2M\hbar\omega_0}}{\hbar K \sqrt{1-G_{ex2}}} + \frac{\hbar^3 K^3(1-G_{ex2})^{3/2} + M\hbar\omega_0 \hbar K \sqrt{1-G_{ex2}}}{2(\hbar^2 K^2(1-G_{ex2}) + 2M\hbar\omega_0)^{3/2}} \right], \quad (16)$$

$$I_K^- \approx \pi \left[\frac{2\hbar^2 K^2(1-G_{ex2}) - 2M\hbar\omega_0}{\hbar^2 K^2(1-G_{ex2})} + \frac{2(M\hbar\omega_0)^2 - M\hbar\omega_0 \hbar^2 K^2(1-G_{ex2})}{2\hbar^4 K^4(1-G_{ex2})^2} \right]. \quad (17)$$

Therefore, the relaxation time for the exciton-polaron is obtained since I_K^+ and I_K^- are determined analytically according to Eq. (13).

B. Electrical conductivity and Seebeck coefficient

The electrical conductivity evaluates the motion of charge carriers in TMDC materials responsible for the current. As for each semiconductor, applying an external field modifies this property. Based on the relaxation-time approximation, the electrical conductivity is given by [57]

$$\sigma_{el} = e^2 \int \Lambda(E) \left(-\frac{\partial f}{\partial E} \right) dE, \quad (18)$$

where $\Lambda(E)$ is the transport function taken as

$$\Lambda(E) = \frac{1}{S} \sum_K v_g^2 \tau \delta(E - E_K). \quad (19)$$

v_g corresponds to the group velocity [58] obtained as

$$v_g = \frac{\hbar K(1-G_{ex2})}{M}. \quad (20)$$

After the integration over K , one gets

$$\Lambda = \frac{(1-G_{ex2})K_0^2}{2\pi M} \{ \tau(K_0) - \tau(-K_0) \}, \quad (21)$$

with

$$K_0 = \frac{\sqrt{2Md}}{\hbar\sqrt{1-G_{ex2}}}; \quad (22)$$

$$d = E + E_b + G_{ex1} - E_g - \xi_B + \xi_{el}.$$

Then, substituting the latest relations in Eq. (18), the electrical conductivity reads

$$\sigma_{el} = \frac{32\eta u \hbar^4 (1-G_{ex2})^3}{\pi M^3 (D_c^{op} - D_v^{op})^4} \beta e^2 \int_0^\infty dE \frac{(d - \hbar\omega_0)\sqrt{d}}{\gamma^2 - \chi^2} f(E), \quad (23)$$

where

$$\gamma = [n_B + f(E + \hbar\omega_0)] \left(\frac{8d^2 + 9\hbar\omega_0 d + 4(\hbar\omega_0)^2}{(d + \hbar\omega_0)^{3/2}} \right) + 2[1 + n_B - f(E - \hbar\omega_0)] \left(\frac{5d - \hbar\omega_0}{\sqrt{d - \hbar\omega_0}} \right), \quad (24)$$

and

$$\chi = 4[1 + n_B - f(E - \hbar\omega_0)] \left(\frac{\hbar\omega_0 - d}{\sqrt{d}} \right). \quad (25)$$

Since the electrical conductivity depends on temperature, it is convenient to explore the Seebeck effect (or thermoelectric power) which evaluates the electric current generated by a gradient of temperature. The Seebeck coefficient takes the form [59]

$$S = \frac{\beta C_1}{e C_2}, \quad (26)$$

where

$$C_1 = \int_0^\infty dE \frac{(d - \hbar\omega_0)\sqrt{d}}{\gamma^2 - \chi^2} f(E)(E - E_F)$$

$$C_2 = \int_0^\infty dE \frac{(d - \hbar\omega_0)\sqrt{d}}{\gamma^2 - \chi^2} f(E). \quad (27)$$

C. Optical conductivity and oscillator strength

The optical conductivity represents the optical response of the TMDC materials and it can be expressed through the Kubo formula [60] at zero temperature by

$$\sigma_{(\omega)} = i \frac{2e^2}{SM\omega} + \frac{1}{S\hbar\omega} \int_0^\infty dt e^{i\omega t} \langle [J(t), J(0)] \rangle. \quad (28)$$

J is the total current operator. Taking into account the electron- and hole-current operators [61], $\sigma_{(\omega)}$ becomes

$$\sigma_{(\omega)} = i \frac{2e^2}{SM\omega} + \frac{1}{S\hbar\omega} \int_0^\infty dt e^{i\omega t} \left\langle \frac{e^2}{m_h^2} [p_h(t), p_h(0)] + \frac{e^2}{m_e^2} [p_e(t), p_e(0)] \right\rangle. \quad (29)$$

After integrating by parts [60], one gets

$$\sigma_{(\omega)} = i \frac{2e^2}{SM\omega} - \frac{e^2}{S\hbar\omega \omega^2} \int_0^\infty dt e^{i\omega t} \left\langle \frac{1}{m_e^2} [F_e(t), F_e(0)] + \frac{1}{m_h^2} [F_h(t), F_h(0)] \right\rangle. \quad (30)$$

As shown in Appendix C, we evaluate the commutators of Eq. (30) and the average is done with respect

to the ground state. We get

$$\begin{aligned} \sigma_{(\omega)} = & i \frac{2e^2}{SM\omega} + \frac{e^2}{S\hbar\omega} \frac{1}{\omega^2} \int_0^\infty dt e^{i\omega t} \left\{ -i \sum_q \left(\frac{e^2 B^2 (m_e^3 + m_h^3)}{2m_e^3 m_h^3} - \frac{eE_{el}(m_h^2 - m_e^2)}{2m_e^2 m_h^2} \right) q \Xi(q) (f_{ex}^* - f_{ex}) \right. \\ & \left. + i \sum_q \left(\frac{e^2 B^2 (m_e^3 + m_h^3)}{2m_e^3 m_h^3} - \frac{eE_{el}(m_h^2 - m_e^2)}{2m_e^2 m_h^2} \right) q \Xi(q) (U(t) f_{ex}^* - T(t) f_{ex}) + \frac{(m_h^2 + m_e^2)}{m_e^2 m_h^2} \sum_q q^2 \Xi^2(q) (U(t) - T(t)) \right\}. \end{aligned} \quad (31)$$

The imaginary part of the optical conductivity is obtained after integrating over t as

$$\text{Im} [\sigma(\omega)] = \frac{2e^2}{SM\omega} + \frac{\hbar e^2 (m_h^2 + m_e^2)}{S\hbar\omega m_e^2 m_h^2 \omega^2} \sum_q q^2 \Xi^2(q) \left(\frac{1}{\lambda_{K+q} - \lambda_K + \hbar\omega - \hbar\omega_0} - \frac{1}{\lambda_{K+q} - \lambda_K + \hbar\omega + \hbar\omega_0} \right). \quad (32)$$

It is seen that the imaginary part represents the optical conductivity out of any field. For the present case in which we investigate the effect of fields, we will focus on the real part. It reads

$$\begin{aligned} \text{Re} [\sigma_{(\omega)}] = & \frac{e^2}{S\hbar\omega} \frac{1}{\omega^2} \left\{ \frac{1}{\omega} \sum_{q//} \left(\frac{e^2 B^2 (m_e^3 + m_h^3)}{2m_e^3 m_h^3} - \frac{eE_{el}(m_h^2 - m_e^2)}{2m_e^2 m_h^2} \right) q \Xi(q) (f_{ex}^* - f_{ex}) \right. \\ & \left. + \hbar \sum_q \left(\frac{e^2 B^2 (m_e^3 + m_h^3)}{2m_e^3 m_h^3} - \frac{eE_{el}(m_h^2 - m_e^2)}{2m_e^2 m_h^2} \right) q \Xi(q) \left(\frac{f_{ex}}{\lambda_{K+q} - \lambda_K + \hbar\omega + \hbar\omega_0} - \frac{f_{ex}^*}{\lambda_{K+q} - \lambda_K + \hbar\omega - \hbar\omega_0} \right) \right\}. \end{aligned} \quad (33)$$

The final expression of the real part of optical conductivity is determined by replacing the summation into integration. It takes the form

$$\text{Re} [\sigma(\omega)] = \sigma_B(\omega) - \sigma_{el}(\omega), \quad (34)$$

with

$$\begin{aligned} \sigma_B(\omega) = & \frac{e^2 (D_c^{\text{op}} - D_v^{\text{op}})^2 \hbar^3 (m_e^3 + m_h^3)}{16S\eta\mu\pi^2 \hbar\omega m_e^3 m_h^3 \omega^2 l_B^2} \int_0^\infty dq \int_0^{2\pi} d\theta q^3 \left\{ \frac{1/\omega}{\frac{\hbar^2 q^2}{2M} + \frac{\hbar^2}{M} Kq \cos \theta - \hbar\omega_0} - \frac{1/\omega}{\frac{\hbar^2 q^2}{2M} + \frac{\hbar^2}{M} Kq \cos \theta + \hbar\omega_0} \right. \\ & + \frac{\hbar}{\left(\frac{\hbar^2 q^2}{2M} + \frac{\hbar^2}{M} Kq \cos \theta + \hbar\omega + \hbar\omega_0 \right) \left(\frac{\hbar^2 q^2}{2M} + \frac{\hbar^2}{M} Kq \cos \theta - \hbar\omega_0 \right)} \\ & \left. - \frac{\hbar}{\left(\frac{\hbar^2 q^2}{2M} + \frac{\hbar^2}{M} Kq \cos \theta + \hbar\omega - \hbar\omega_0 \right) \left(\frac{\hbar^2 q^2}{2M} + \frac{\hbar^2}{M} Kq \cos \theta + \hbar\omega_0 \right)} \right\}, \end{aligned} \quad (35)$$

and

$$\begin{aligned} \sigma_{el}(\omega) = & \frac{e^3 (D_c^{\text{op}} - D_v^{\text{op}})^2 (m_h^2 - m_e^2) E_{el}}{16S\eta\mu\pi^2 m_e^2 m_h^2 \omega^3} \int_0^\infty dq \int_0^{2\pi} d\theta q^3 \left\{ \frac{1/\omega}{\frac{\hbar^2 q^2}{2M} + \frac{\hbar^2}{M} Kq \cos \theta - \hbar\omega_0} - \frac{1/\omega}{\frac{\hbar^2 q^2}{2M} + \frac{\hbar^2}{M} Kq \cos \theta + \hbar\omega_0} \right. \\ & + \frac{\hbar}{\left(\frac{\hbar^2 q^2}{2M} + \frac{\hbar^2}{M} Kq \cos \theta + \hbar\omega + \hbar\omega_0 \right) \left(\frac{\hbar^2 q^2}{2M} + \frac{\hbar^2}{M} Kq \cos \theta - \hbar\omega_0 \right)} \\ & \left. - \frac{\hbar}{\left(\frac{\hbar^2 q^2}{2M} + \frac{\hbar^2}{M} Kq \cos \theta + \hbar\omega - \hbar\omega_0 \right) \left(\frac{\hbar^2 q^2}{2M} + \frac{\hbar^2}{M} Kq \cos \theta + \hbar\omega_0 \right)} \right\}. \end{aligned} \quad (36)$$

Now that the optical conductivity is obtained, let us evaluate the strength of optical transitions by the formula [62]

$$F_{osc}(\omega) = \frac{2\pi \varepsilon_0 M}{ne^2 \omega^2} \frac{1}{\tau_l}. \quad (37)$$

F_{osc} is the oscillator strength and τ_l is the ground-state exciton-polaron lifetime taken as [63]

$$\frac{1}{\tau_l} = \frac{2\pi}{\hbar} \sum_q | \langle n_q, K | H_{ex-ph}^{2D} | K, n_q \rangle |^2 \delta[\lambda_K - \lambda_{K+q} + \hbar\omega_0]. \quad (38)$$

TABLE I. Characteristics of each TMDC taken from Refs. [14,65].

	m_e (m_0)	m_h (m_0)	$\hbar\omega_0$ (eV)	D_c^{op} (eV)	D_v^{op} (eV)	E_b (eV)	E_g (eV)
MoSe ₂	0.64	0.71	0.0365	5.2	4.9	0.174	1.56
WSe ₂	0.39	0.51	0.0291	2.3	3.1	0.231	1.65
WS ₂	0.31	0.42	0.0435	3.1	2.3	0.19	2.10
MoS ₂	0.51	0.58	0.0443	5.8	4.6	0.313	1.87

Here we consider $n_q = n_q - 1$ and the summation is transformed into integration. The integration over q , after averaging with $|\Psi_0\rangle$, gives

$$\frac{1}{\tau_l} = \frac{M(D_c^{\text{op}} - D_v^{\text{op}})^2}{\hbar^3 \pi \eta u} \bar{N}_0 \int_0^{2\pi} d\theta \frac{(\hbar^2 K^2 \cos^2 \theta + M\hbar\omega_0)}{\sqrt{\hbar^2 K^2 \cos^2 \theta + 2M\hbar\omega_0}}, \quad (39)$$

where \bar{N}_0 is the mean number of phonons [64] and the final expression of the oscillator strength is determined by substituting the latest relation in Eq. (37). This leads to

$$F_{\text{osc}} = \frac{2\varepsilon_0(D_c^{\text{op}} - D_v^{\text{op}})^2 M^2}{n\eta u e^2 \hbar^3} \frac{1}{[\exp(\beta E_K) - 1] \omega^2} \times \int_0^{2\pi} d\theta \frac{(\hbar^2 K^2 \cos^2 \theta + M\hbar\omega_0)}{\sqrt{\hbar^2 K^2 \cos^2 \theta + 2M\hbar\omega_0}}. \quad (40)$$

From Eqs. (13), (23), (26), (34), and (40) it is clear that the relaxation time, the electrical conductivity, the Seebeck coefficient, the optical conductivity, and the oscillator strength calculated for 1Ls TMDCs are influenced by both the magnetic barrier and the electric field acting on the TMDC monolayer.

III. RESULTS AND DISCUSSION

For calculations of the properties we have described above, we use the following data showing some materials characteristics (see Table I).

Figures 2 and 3 plot the variation of the exciton-polaron ground-state energy for various monolayers TMDCs. Figure 2

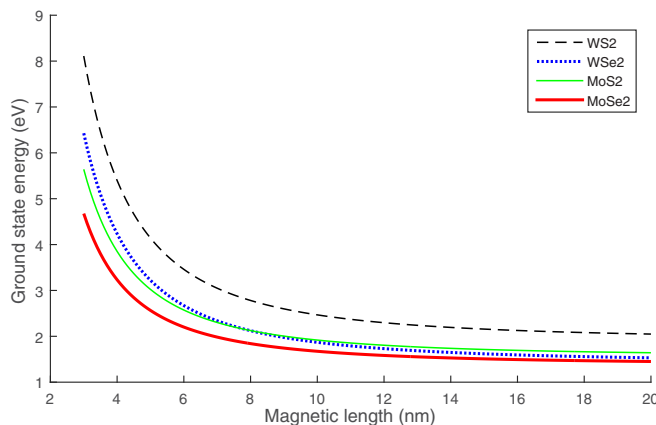


FIG. 2. GS energy of exciton-polaron as function of the magnetic length for zero electric field.

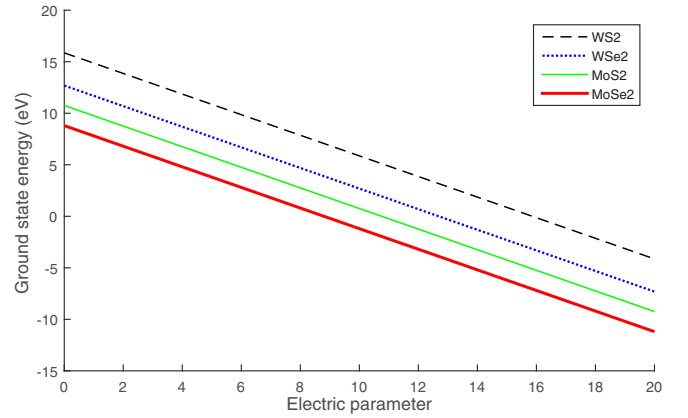


FIG. 3. GS energy of exciton-polaron vs the electric parameter for $l_B = 2$ nm.

shows the decrease of the exciton-polaron energy when enhancing the magnetic length and one can say that the energy is sensitive to the applied magnetic barrier.

Since the magnetic strength is inversely proportional to the magnetic length, it follows that the excitonic polaron energy increases with the enhancement of the magnetic field. In fact, the magnetic field reduces the interparticle distance and increases the Coulomb interaction of the electron-hole pair [41]. This leads to the increase of the binding energy. The excitonic polaron is then confined in the magnetic barrier and that favors its stability. Also, for $l_B > 15$ nm the energy becomes constant, meaning that the magnetic barrier loses its influence and it corresponds to weak magnetic range.

However, from the curves of Fig. 3, we observe a monotonic decrease of the GS energy when the electric parameter increases. Even if the excitonic polaron is a neutral set, it remains a two-particle system of opposite charges and then the presence of electric field affects the excitonic components.

In fact, the hole tends to move in the electric field direction, whereas its corresponding electron moves against the electric field. Because of this opposition in direction, one can say that due to the applied electric field the binding energy is reduced and it brings down the excitonic polaron stability. It adheres with the work of Oukerroum *et al.* [66]; Ref. [50] predicts the dissociation of exciton by electric field. The highest GS energy is obtained in WS₂ and the lowest in MoSe₂.

Figures 4 and 5 show the relaxation time of the exciton-polaron as a function of the magnetic length (l_B) and the electric parameter (ξ_{el}) respectively. The result indicates that the relaxation time increases as the magnetic length and electric parameter increase, and it saturates for high values of the parameters.

The relaxation of exciton-polaron is related to the process of phonons' absorption-emission in TMDCs. This process is influenced by the interaction with phonons: the less the exciton interacts in the structure, the more it relaxes. In fact, from the results of GS energy, it is shown that the enhancement of the magnetic length leads to the reduction in exciton binding energy. As the binding energy decreases, the interplay between exciton and phonon is lowered. This justifies the increase of the relaxation time observed in Fig. 4 and it adheres with Ref. [67]. In addition, it is observed that the

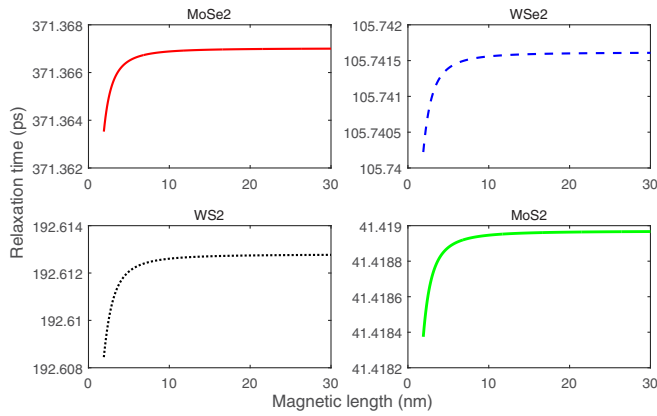


FIG. 4. Exciton-polaron relaxation time vs the magnetic length at $T = 70$ K.

saturation occurs at $l_B = 15$ nm, meaning that the exciton-polaron reaches its maximum relaxation time and one can say that the phenomenon of relaxation is sensitive to the magnetic barrier. In the same way, as the electric field is applied, it delocalizes the hole and electron toward different directions. This generates the decrease of exciton binding energy contributing to the reduction of particle interactions. Therefore, the electron and hole are more relaxed in the presence of an external electric field and the exciton-polaron relaxation time enhances as shown in Fig. 5. The lowest relaxation time is observed in MoS₂ and the highest in MoSe₂. Also, Yan *et al.* [68] used a spectroscopic method in WSe₂ and found the relaxation time of free exciton about 2 ps at 70 K. Here, the relaxation time for WSe₂ is about 105 ps. Thus, we predict that the relaxation time of exciton-polaron in the presence of electric field and magnetic barrier is 50 times larger than that of free exciton.

Figures 6 and 7 present the electrical conductivity for TMDCs as a function of the magnetic length and electric parameter, respectively. One can see from Eq. (23) that the electrical conductivity is proportional to \sqrt{d} and according to Eq. (22), we have $\sqrt{d} = \sqrt{E + E_b + G_{ex1} - E_g}$ when the fields are zero. Then, in the absence of any field, the electrical conductivity appears when the system's energy overpasses the

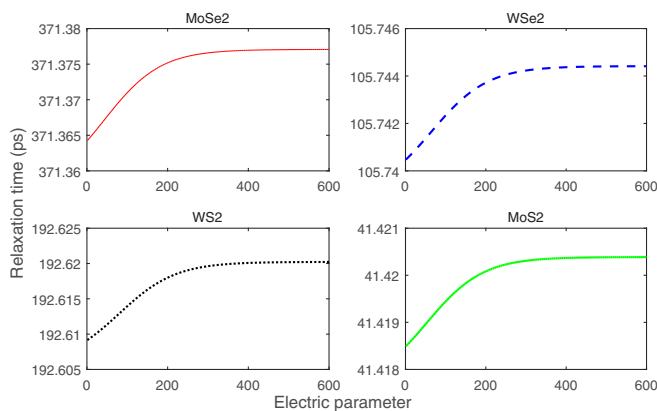


FIG. 5. Exciton-polaron relaxation time vs the electric parameter at $T = 70$ K.

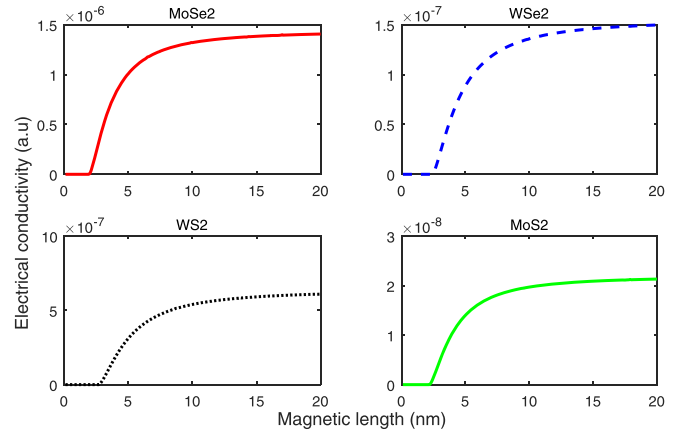


FIG. 6. Electrical conductivity vs the magnetic length at $T = 25$ K.

band-gap energy, so that the electron can transit toward the conduction band.

Now from Fig. 6, it follows that there is no electrical conductivity for low values of the magnetic length. This result indicates that at very high magnetic strength, there is no electrical conductivity in TMDCs. Moreover, the system's energy should be greater than the band gap and the magnetic parameter since the electrical conductivity becomes proportional to $\sqrt{E + E_b + G_{ex1} - E_g - \xi_B}$ according to Eq. (22).

As the magnetic length increases, it favors the attenuation of the magnetic strength, and the electrical conductivity becomes possible. This occurs when the magnetic length reaches a value around 2.5 nm and from this value the electrical conductivity increases as the magnetic length increases. This enhancement of the electrical conductivity is in accordance with Refs. [69,70]. Also, applying the magnetic field along the z direction induces the confinement and carriers' concentration in the xy plane. Then, as l_B increases, electron- and hole interactions with phonons grow because the particles motion increases. In Ref. [71] it is shown that the polaron motion is fast with higher magnetic barrier lengths.

Figure 7 shows the enhancement of electrical conductivity when the electric parameter increases. Reference [50]

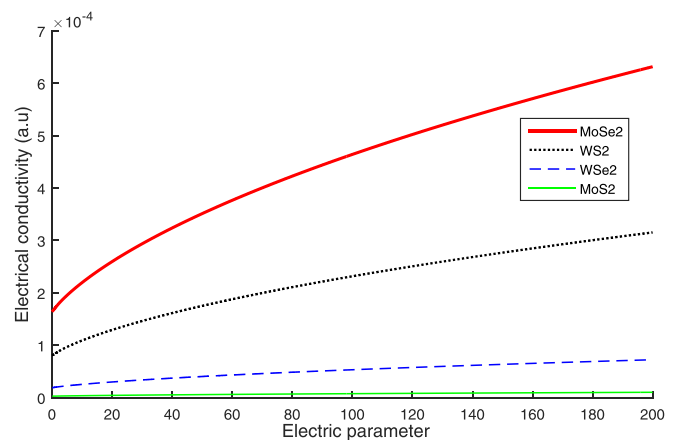


FIG. 7. Electrical conductivity vs the electric parameter at $T = 25$ K.

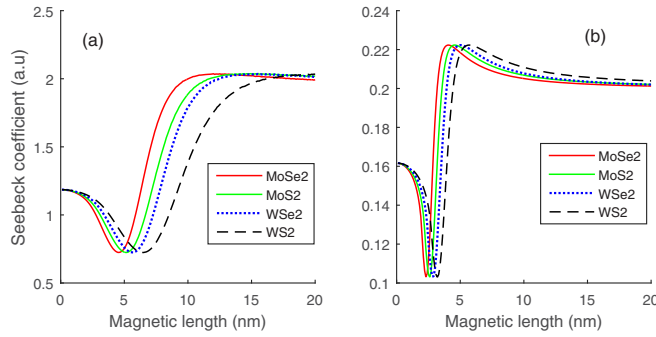


FIG. 8. Seebeck coefficient vs the magnetic length for (a) $T = 5$ K and (b) $T = 150$ K.

demonstrated that the exciton energy level decreases when the electric field increases. In addition, the applied electric field induces an electric force responsible for the increase of electron's motion in TMDCs. Thus, the electric field facilitates the electronic transitions and it agrees with Ref. [72]. In addition, Fig. 7 shows a very low electrical conductivity in MoS₂ for $\xi_{el} = 0$ ($E_{el} = 0$) at 25 K. This is a good result, adhering with the experiment of Kim *et al.* [73]. The latest observed the increase of electrical conductivity with temperature and a weak value (close to zero) in 1L MoS₂ without heterostructure at 300 K.

Among the selected TMDCs, MoSe₂ has the greatest amplitude and its electrical conductivity begins at a low value ($l_B \approx 2$ nm), meaning that it is a suitable TMDC for studies in high magnetic fields. This can be due to its lowest band-gap energy which favors the electronic transition between valence- and conduction bands. This result of MoSe₂, also suggested by Figs. 4 and 5, fits with Ref. [42], which showed that the electrical conductivity rises when the relaxation time increases.

The Seebeck coefficient as a function of the magnetic length for low- and high temperatures and diverse TMDCs is presented in Figs. 8(a) and 8(b), respectively. It is observed that the curves do not present monotonic shapes. The Seebeck coefficient falls until to a critical value of the magnetic length, and above this value it increases. In fact, as the temperature changes in TMDCs, it generates excitations and increases the motion of particles. This leads to the appearance of a voltage responsible for the Seebeck effect. At a fixed temperature and for low values of the magnetic length, which means high magnetic field, the magnetic influence dominates. Then, electron (hole) is more confined than subjected to thermal perturbation and it explains the decrease of this property.

In the opposite way, above the critical value of the magnetic length, which means low magnetic field, the temperature effect dominates and enhances the Seebeck coefficient. It is in agreement with Refs. [70,74].

Also, the result shows that the magnetic effect is less significant in high-temperature range since one can observe the regression of the critical value range [from 5–7 nm in Fig. 8(a) to 2.5–3.5 nm in Fig. 8(b)] and the reduction of the Seebeck coefficient values regarding Fig. 8(a) and Fig. 8(b). In addition, for very high values of the magnetic length ($l_B > 18$ nm) in Fig. 8(a) and $l_B > 10$ nm in Fig. 8(b)), the Seebeck

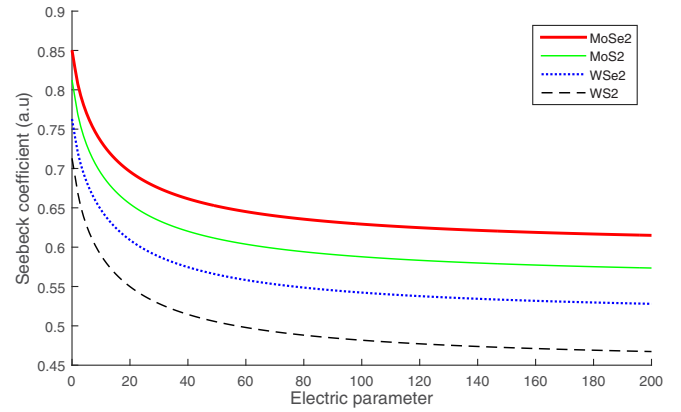


FIG. 9. Seebeck coefficient vs the electric parameter at $T = 25$ K.

coefficient becomes constant and the magnetic barrier does not influence this property more. At $T = 5$ K, the highest amplitude is obtained for WS₂ at low magnetic length and for MoSe₂ at high magnetic length.

Figure 9 presents the evolution of the Seebeck coefficient of TMDCs in the presence of the external electric field. The result shows the highest amplitudes of the coefficient at zero electric field. It decreases gradually as the field increases. This decrease of S_b is in agreement with Ref. [75] and the experiment of Ref. [76]. Thus, the Seebeck effect as a thermoelectric power property is favored by the absence of the electric field. In this case, when the temperature changes, the electron (hole) moves directed only by the temperature gradient from the hot source to the cold source, and then it generates the Seebeck voltage.

In the presence of the electric field, the particles' motion is governed by the field. As the strength of the electric field increases, it overcomes the temperature gradient and the curves of the Seebeck coefficient decrease.

Figures 10 and 11 present the real part of the optical conductivity of TMDCs versus the magnetic length and electric field, respectively. The optical conductivity of TMDCs presents a high amplitude and this is also observed at room temperature by Kravets *et al.* [77]. The figures show that this

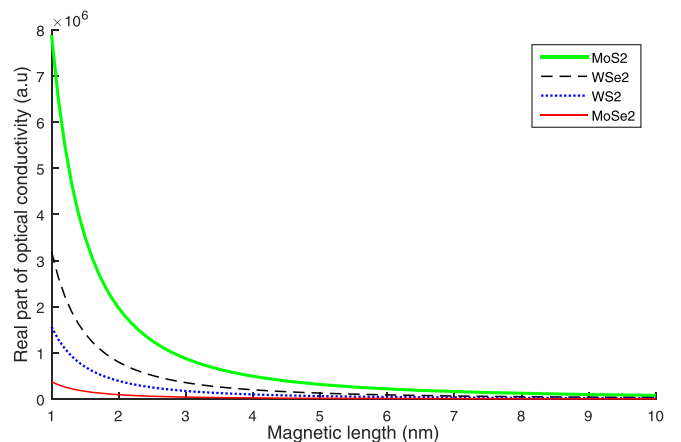


FIG. 10. Real part of the optical conductivity vs the magnetic length at $\hbar\omega = 0.1$ eV and $E_{el} = 0$.

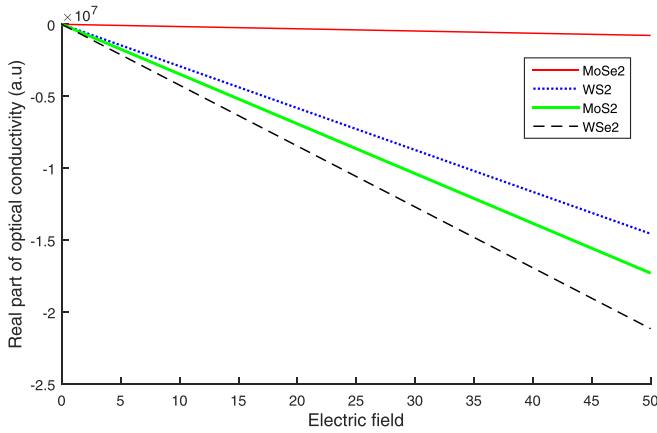


FIG. 11. Real part of optical conductivity vs the electric field for $l_B = 2$ nm and $\hbar\omega = 0.1$ eV.

property decreases when the magnetic length and electric field increase. It adheres, respectively, with Refs. [61,49]. As the applied energy $\hbar\omega$ is more than twice the phonon energy, the exciton-polaron becomes more energetic and then optical transitions can occur [55,78].

Moreover, the particles are well confined in the presence of the magnetic barrier favoring the growth of their energies. The increase of the magnetic length has the effect of reduce the exciton-polaron energy, then decreasing the optical conductivity as pointed out in Fig. 10. The highest optical conductivity is obtained for MoS₂.

Also, the presence of the electric field modifies the Coulomb force between electrons and holes reducing the exciton binding energy. In addition, according to Eq. (10) it is seen that the increase of the electric field leads to the decrease of the system energy. Therefore, the electric field does not favor the optical transitions. The negative sign in Fig. 11 is justified by the dominance of the electric field effect against the magnetic barrier according to Eq. (34).

Figures 12 and 13, respectively, show the evolution of the excitonic polaron oscillator strength when the magnetic length and the electric parameter change. The results indicate that it increases with the magnetic length and electric field. One can say that this property is very sensitive to low magnetic lengths

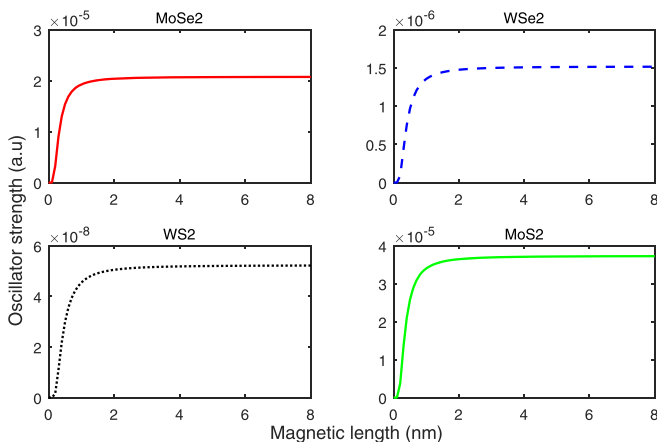


FIG. 12. Oscillator strength vs the magnetic length at $T = 25$ K.

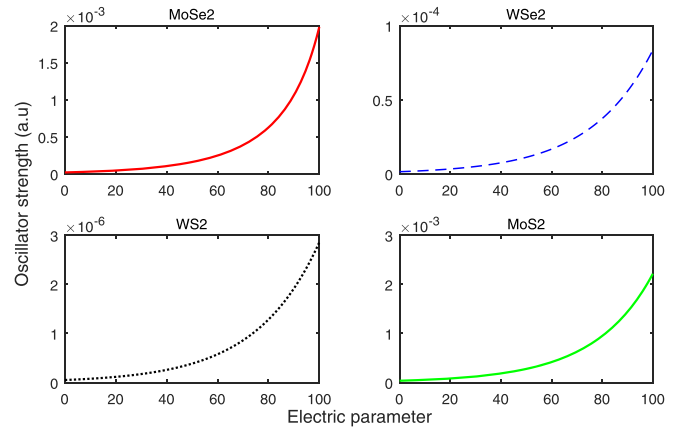


FIG. 13. Oscillator strength vs the electric parameter at $T = 25$ K.

(high magnetic strength) due to the rapid growth observed in Fig. 12.

From Eq. (37), it is seen that the lifetime is inversely proportional to the oscillator strength. The curve presents a saturation when $l_B > 2$ nm; the oscillator strength reaches its maximum and becomes constant. This range also corresponds to the shortest lifetime characterizing the lowest stability of exciton-polaron, since when the lifetime is zero it means the death of this quasiparticle [54]. Hence, the result shows that the less the exciton is confined, the lower its lifetime, the greater the oscillator strength, and it joins the work of Ref. [79]. From Fig. 13, it is seen that as the electric field increases, the particles' motions grow and the optical transition is faster. Moreover, it is in agreement with Ref. [72] which shows the decrease of lifetime when the electric field rises. Among the TMDCs, the highest value of oscillator strength is observed in MoS₂.

IV. CONCLUSION

The relaxation of exciton-polaron and the transport properties under a magnetic barrier and an electric field have been investigated in various TMDCs. The analytical study of the relaxation time, the electrical conductivity, the Seebeck coefficient, the optical conductivity, and the oscillator strength has been done. It follows that the relaxation time of the exciton-polaron grows when the magnetic length and electric field increase. Also, the electrical conductivity increases as the magnetic length and electric field increase. It reaches at different values of the magnetic length characterizing each TMDC material. In addition, the Seebeck coefficient presents a monotonic decrease under the electric field, whereas the magnetic barrier changes its behavior. The low values of the magnetic length favor the decrease of this coefficient while the high values increase it. Moreover, the optical conductivity of TMDCs decreases with increasing both the magnetic length and electric field. The oscillator strength of the excitonic polaron is an increasing function of both magnetic length and electric field. It increases gradually as the electric field increases. This work shows that the magnetic barrier and the electric field can be used to adjust these transport properties and relaxation of the exciton-polaron in TMDCs. This could be useful to improve optical- and electronic device properties.

ACKNOWLEDGMENTS

This research was supported by the Deutscher Akademischer Austauschdienst German Academic Exchange Service through the Staff Exchange Fellowships in Sub-Saharan-Africa under the funding Programme No. 57588199. N.C. acknowledges also support from ANID Fondecyt Iniciación en Investigación Project No. 11221088.

APPENDIX A: DIAGONALIZATION METHOD

Let us use the unitary transformation:

$$U_{ex} = \exp(iS_a), \quad (\text{A1})$$

with

$$S_a = \sum_{K,q} C_{K+q}^+ C_K [f_{ex}^* b_{-q}^+ + f_{ex} b_q]. \quad (\text{A2})$$

The f_{ex} functions are variational parameter. We apply the unitary transformation to the full Hamiltonian and get

$$\hat{\Gamma} = U_{ex}^{-1} \hat{H} U_{ex} \approx \hat{H}_{ex}^{2D} + \hat{H}_{ph} + \hat{\Gamma}_{ex-ph}^{2D}. \quad (\text{A3})$$

The transformed Hamiltonian can be separated as

$$\hat{\Gamma} = \hat{H}_0 + \hat{\Gamma}_{ex-ph}^{2D}, \quad (\text{A4})$$

where the free part \hat{H}_0 and the interacting part $\hat{\Gamma}_{ex-ph}^{2D}$ of $\hat{\Gamma}$ are given by

$$\hat{H}_0 = \hat{H}_{ex}^{2D} + \hat{H}_{ph}, \quad (\text{A5})$$

$$\hat{\Gamma}_{ex-ph}^{2D} = \sum_{K,K',q} |\Xi^{\text{op}}(q)|^2 (f_{ex}^* - f_{ex}) C_{K+q}^+ C_K C_{K'+q}^+ C_{K'}. \quad (\text{A6})$$

Using a series expansion of (A4) and the perturbation theory [14], we obtain the f_{ex} functions as

$$f_{ex}^* = \frac{\Xi^{\text{op}}(q)}{\lambda(K+q, l_B, E_{el}) - \lambda(K, l_B, E_{el}) + \hbar\omega_0}$$

$$f_{ex} = \frac{\Xi^{\text{op}}(q)}{\lambda(K+q, l_B, E_{el}) - \lambda(K, l_B, E_{el}) - \hbar\omega_0}. \quad (\text{A7})$$

Therefore, according to (A7) and Eq. (6), we evaluate the summation over q in (A6). This leads to

$$\hat{\Gamma}_{ex-ph}^{2D} = - \sum_{K,K'} [\tilde{G}_{ex2} + G_{ex1}] C_{K+q}^+ C_K C_{K'+q}^+ C_{K'}, \quad (\text{A8})$$

with

$$G_{ex1} = \frac{\pi \sqrt{\hbar\omega_0} (D_c^{\text{op}} - D_v^{\text{op}})^2}{\sqrt{2} \hbar^2 \eta u} (m_e + m_h)^{3/2}, \quad (\text{A9})$$

APPENDIX C: COMMUTATOR OF FORCE OPERATORS AND AVERAGING

The force operator is defined as $F_\alpha(t) = (i/\hbar)[H, p_\alpha]$, with the linear momentum operator taken in the second quantization as $p_\alpha = \hbar K_\alpha C_{K\alpha}^+ C_{K\alpha}$ [60], α standing for electron (e) or hole (h).

Thus,

$$F_e(t) = -i \left\{ \left(\frac{e^2 B^2}{2m_e} - eE_{el} \right) C_{Ke}^+(t) C_{Ke}(t) + \sum_q q \Xi(q) C_{K+q}^+(t) C_K(t) (b_q(t) + b_{-q}^+(t)) \right\}, \quad (\text{C1})$$

$$\tilde{G}_{ex2} = \left(\frac{\hbar^2 K^2}{2M} \right) \frac{3\pi (D_c^{\text{op}} - D_v^{\text{op}})^2 (m_e + m_h)^{3/2}}{4\sqrt{2} \hbar^2 \eta u \sqrt{\hbar\omega_0}}$$

$$= \left(\frac{\hbar^2 K^2}{2M} \right) G_{ex2}. \quad (\text{A10})$$

Thus, the Hamiltonian in its approximate diagonalized form, taking into account Eq. (7), becomes

$$\hat{\Gamma} = \sum_K \lambda C_K^+ C_K + \hat{H}_{ph} - \sum_{K,K'} [\tilde{G}_{ex2} + G_{ex1}] C_{K+q}^+ C_K C_{K'+q}^+ C_{K'}. \quad (\text{A11})$$

APPENDIX B: DEVELOPMENT OF THE DIRAC DELTA FUNCTION

Let us use the following relation:

$$\delta[g(q)] = \sum_i \frac{\delta(q - q_i)}{|g'(q_i)|}, \quad (\text{B1})$$

where q_i are the roots of the g functions contained in the Dirac delta function and g' its derivative. From Eq. (12), we consider

$$g_1 = E_K - E_{K+q} + \hbar\omega_0, \quad (\text{B2})$$

$$g_2 = E_K - E_{K+q} - \hbar\omega_0. \quad (\text{B3})$$

According to Eqs. (10) and (B1), we establish

$$\delta(g_1) = \frac{M}{\hbar^2 (1 - G_{ex2})} \frac{\delta(q - q_1) + \delta(q - q_2)}{\sqrt{K^2 \cos^2 \theta + 2M\hbar\omega_0/\hbar^2 (1 - G_{ex2})}}, \quad (\text{B4})$$

$$\delta(g_2) = \frac{M}{\hbar^2 (1 - G_{ex2})} \frac{\delta(q - q_3) + \delta(q - q_4)}{\sqrt{K^2 \cos^2 \theta - 2M\hbar\omega_0/\hbar^2 (1 - G_{ex2})}}, \quad (\text{B5})$$

with

$$q_1 = -K \cos \theta + \sqrt{K^2 \cos^2 \theta + 2M\hbar\omega_0/\hbar^2 (1 - G_{ex2})}$$

$$q_2 = -K \cos \theta - \sqrt{K^2 \cos^2 \theta + 2M\hbar\omega_0/\hbar^2 (1 - G_{ex2})}, \quad (\text{B6})$$

$$q_3 = -K \cos \theta + \sqrt{K^2 \cos^2 \theta - 2M\hbar\omega_0/\hbar^2 (1 - G_{ex2})}$$

$$q_4 = -K \cos \theta - \sqrt{K^2 \cos^2 \theta - 2M\hbar\omega_0/\hbar^2 (1 - G_{ex2})}. \quad (\text{B7})$$

These expressions (B4) and (B5) of the Dirac delta functions are suitable for integration or summation.

$$F_h(t) = -i \left\{ \left(\frac{e^2 B^2}{2m_h} + eE_{el} \right) C_{Kh}^+(t) C_{Kh}(t) + \sum_q q \Xi(q) C_{K+q}^+(t) C_K(t) (b_q(t) + b_{-q}^+(t)) \right\}. \quad (C2)$$

Also, the time dependence of the operators is given by

$$b_q(t) = e^{-i\omega_0 t} b_q(0); \quad b_{-q}^+(t) = e^{i\omega_0 t} b_{-q}^+(0), \quad (C3)$$

and

$$\begin{aligned} C_{K\alpha}^+(t) C_{K\alpha}(t) &= e^{(it/\hbar)\lambda_K} C_{K\alpha}^+(0) e^{[-(-it)/\hbar]\lambda_K} C_{K\alpha}(0) \\ C_{K+q}^+(t) C_K(t) &= e^{(it/\hbar)\lambda_{K+q}} C_{K+q}^+(0) e^{[-(-it)/\hbar]\lambda_K} C_K(0). \end{aligned} \quad (C4)$$

After straightforward calculations made in Eq. (30), we evaluate the commutator taking into account (C1), (C2), and the time dependence of the operators. This leads to

$$\begin{aligned} \left\langle \frac{1}{m_e^2} [F_e(t), F_e(0)] + \frac{1}{m_h^2} [F_h(t), F_h(0)] \right\rangle &= \left\langle \left\{ \sum_q \left(\frac{e^2 B^2 (m_e^3 + m_h^3)}{2m_e^3 m_h^3} - \frac{eE_{el} (m_h^2 - m_e^2)}{2m_e^2 m_h^2} \right) q \Xi(q) C_{K+q}^+ C_K (b_q + b_{-q}^+) \right. \right. \\ &\quad - \sum_q \left(\frac{e^2 B^2 (m_e^3 + m_h^3)}{2m_e^3 m_h^3} - \frac{eE_{el} (m_h^2 - m_e^2)}{2m_e^2 m_h^2} \right) q \Xi(q) C_{K+q}^+ C_K (U(t)b_q + T(t)b_{-q}^+) \\ &\quad \left. \left. - \frac{(m_h^2 + m_e^2)}{m_e^2 m_h^2} \sum_q q^2 \Xi^2(q) C_{K+q}^+ C_K C_{K+q}^+ C_K (U(t) - T(t)) \right\} \right\rangle, \end{aligned} \quad (C5)$$

where

$$\begin{aligned} T(t) &= \exp \frac{it}{\hbar} (\lambda_{K+q} - \lambda_K + \hbar\omega_0); \\ U(t) &= \exp \frac{it}{\hbar} (\lambda_{K+q} - \lambda_K - \hbar\omega_0). \end{aligned} \quad (C6)$$

We then apply the unitary transformation and obtain

$$\begin{aligned} \left\langle \frac{1}{m_e^2} [F_e(t), F_e(0)] + \frac{1}{m_h^2} [F_h(t), F_h(0)] \right\rangle &= \left\langle \left\{ \sum_q \left(\frac{e^2 B^2 (m_e^3 + m_h^3)}{2m_e^3 m_h^3} - \frac{eE_{el} (m_h^2 - m_e^2)}{2m_e^2 m_h^2} \right) \right. \right. \\ &\quad \times q \Xi(q) C_{K+q}^+ C_K (b_q + b_{-q}^+ + i C_{K+q}^+ C_K (f_{ex}^* - f_{ex})) \\ &\quad - \sum_q \left(\frac{e^2 B^2 (m_e^3 + m_h^3)}{2m_e^3 m_h^3} - \frac{eE_{el} (m_h^2 - m_e^2)}{2m_e^2 m_h^2} \right) \\ &\quad \times q \Xi(q) C_{K+q}^+ C_K (U(t)b_q + T(t)b_{-q}^+ + iU(t)C_{K+q}^+ C_K f_{ex}^* - iT(t)C_{K+q}^+ C_K f_{ex}) \\ &\quad \left. \left. - \frac{(m_h^2 + m_e^2)}{m_e^2 m_h^2} \sum_q q^2 \Xi^2(q) C_{K+q}^+ C_K C_{K+q}^+ C_K (U(t) - T(t)) \right\} \right\rangle. \end{aligned} \quad (C7)$$

The average is done using the ground-state wave function. We have

$$\begin{aligned} \left\langle \frac{1}{m_e^2} [F_e(t), F_e(0)] + \frac{1}{m_h^2} [F_h(t), F_h(0)] \right\rangle &= \left\{ i \sum_q \left(\frac{e^2 B^2 (m_e^3 + m_h^3)}{2m_e^3 m_h^3} - \frac{eE_{el} (m_h^2 - m_e^2)}{2m_e^2 m_h^2} \right) \right. \\ &\quad \times q \Xi(q) (f_{ex}^* - f_{ex}) - i \sum_q \left(\frac{e^2 B^2 (m_e^3 + m_h^3)}{2m_e^3 m_h^3} - \frac{eE_{el} (m_h^2 - m_e^2)}{2m_e^2 m_h^2} \right) q \Xi(q) (U(t)f_{ex}^* \\ &\quad \left. - T(t)f_{ex}) - \frac{(m_h^2 + m_e^2)}{m_e^2 m_h^2} \sum_q q^2 \Xi^2(q) (U(t) - T(t)) \right\}. \end{aligned} \quad (C8)$$

- [1] A. Kormányos, V. Zolyomi, N. D. Drummond, and G. Burkard, Spin-Orbit Coupling Quantum Dots and Qubits in Monolayer Transition Dichalcogenides, *Phys. Rev. X* **4**, 011034 (2014).
- [2] X. X. Song, D. Liu, V. Mosallanejad, J. You, T. Y. Han, D. T. Chen, H. O. Li, G. Cao, M. Xiao, G. C. Guo, and G. P. Guo, A gate defined quantum dot on the two-dimensional transition metal dichalcogenide semiconductor WSe₂, *Nanoscale* **7**, 16867 (2015).
- [3] A. J. Pearce and G. Burkard, Electron spin relaxation in a transition metal dichalcogenide quantum dot, *2D Mater.* **4**, 025114 (2017).
- [4] K. F. Mak, K. He, C. Lee, G. H. Lee, J. Hone, T. F. Heinz, and J. Shan, Observation of tightly trions in monolayer MoS₂, *Nat. Mater.* **12**, 207 (2013).
- [5] D. Y. Qiu, T. Cao, and S. G. Louie, Nonanalyticity Valley Quantum Phases and Lightlike Exciton Dispersion in Monolayer Transition Metal Dichalcogenides: Theory and First Principles Calculations, *Phys. Rev. Lett.* **115**, 176801 (2015).
- [6] L. Yang, C. Xie, J. Jin, R. N. Ali, C. Feng, P. Liu, and B. Xiang, Properties preparation and applications of low dimensional transition metal dichalcogenides, *Nanomaterials* **8**, 463 (2018).
- [7] G. Fiori, F. Bonaccorso, G. Ianncone, T. Palacios, D. Neumaier, A. Seabaugh, S. K. Banerjee, and L. Colombo, Electronics based on two dimensional materials, *Nat. Nanotechnol.* **9**, 768 (2014).
- [8] M. Bernardi, C. Ataca, M. Palumbo, and J. C. Grossman, Optical and electronic properties of two dimensional layered materials, *Nanophotonics* **6**, 479 (2017).
- [9] G. Wang, C. Robert, M. M. Glazov, F. Cadiz, E. Courtade, T. Amand, D. Lagarde, T. Taniguchi, K. Watanabe, B. Urbaszek, and X. Marie, In-plane Propagation of Light in Transition Metal Dichalcogenide Monolayers: Optical Selection Rules, *Phys. Rev. Lett.* **119**, 047401 (2017).
- [10] P. Dey, L. Yang, C. Robert, G. Wang, B. Urbaszek, X. Marie, and S. A. Crooker, Gate Controlled Spin Valley Locking of Resident Carriers in WSe₂ Monolayers, *Phys. Rev. Lett.* **119**, 137401 (2017).
- [11] S. Ono and Tomohiro, Anomalous energy shift of laterally confined two dimensional excitons, *J. Appl. Phys.* **124**, 034301 (2018).
- [12] S. Shree, M. Semina, C. Robert, B. Han, T. Amand, A. Balocchi, M. Manca, E. Courtade, X. Marie, T. Taniguchi, K. Watanabe, M. M. Glazov, and B. Urbaszek, Observation of exciton phonon coupling in MoSe₂ monolayers, *Phys. Rev. B* **98**, 035302 (2018).
- [13] A. Chernikov, T. C. Berkelbach, H. M. Hill, A. Rigosi, Y. Li, Ö. B. Aslan, D. R. Reichman, M. S. Hybertsen, and T. F. Heinz, Exciton Binding Energy and Nonhydrogenic Rydberg Series in Monolayer WS₂, *Phys. Rev. Lett.* **113**, 076802 (2014).
- [14] A. Thilagam, Excitonic polarons in low dimensional transition metal dichalcogenides, *Phys. B: Condens. Matter* **464**, 44 (2015).
- [15] D. Akay, Trigonal warping and photoinduced effects on zone boundary phonon in monolayer graphene, *Superlattices Microstruct.* **117**, 18 (2018).
- [16] B. S. Kandemir and D. Akay, Photoinduced dynamical band gap in graphene: The effects of electron phonon and spin orbit interaction, *Phys. Status Solidi B* **255**, 1800163 (2018).
- [17] I. Favero, G. Cassabois, R. Ferreira, D. Darson, C. Voisin, J. Tignon, C. Delalande, G. Bastard, P. Roussignol, and J. M. Gerard, Acoustic phonon sidebands in the emission line of single InAs/GaAs quantum dots, *Phys. Rev. B* **68**, 233301 (2003).
- [18] B. Krummheuer, V. M. Axt, and T. Kuhn, Theory of pure dephasing and the resulting absorption line shape in semiconductor quantum dots, *Phys. Rev. B* **65**, 195313 (2002).
- [19] P. Machnikowski Jacak, J. Krasnyj, and P. Zoller, Coherent and incoherent phonon processes in artificial atoms, *Eur. Phys. J. D* **22**, 319 (2003).
- [20] V. Jankovic and N. Vukmirovic, Dynamics of exciton formation and relaxation in photoexcited semiconductors, *Phys. Rev. B* **92**, 235208 (2015).
- [21] S. Brem, M. Selig, G. Berghaeuser, and E. Malic, Exciton relaxation cascade in two dimensional transition metal dichalcogenides, *Sci. Rep.* **8**, 8238 (2018).
- [22] V. A. Maidanyk and Y. H. Roos, Modification of the WLF Model for characterization of the relaxation time-temperature relationship in trehalose whey protein isolate systems, *J. Food Eng.* **188**, 21 (2016).
- [23] I. Singh, S. Madan, A. Kaur, J. Kumar, P. K. Bhatnagar, and P. C. Mathur, Study of relaxation dynamics of photogenerated excitons in CuInS₂ quantum dots, *MRS Commun.* **4**, 1 (2014).
- [24] L. Foglia, S. Vempati, B. T. Bonkano, L. Gierster, M. Wolf, S. Sadofev, and J. Stahler, Revealing the competing contributions of charge carriers excitons and defects to the non-equilibrium optical properties of ZnO, *Struct. Dyn.* **6**, 034501 (2019).
- [25] A. O. El-Ballouli, E. Alarousu, A. Usman, J. Pan, O. M. Bakr, and O. F. Mohammed, Real time observation of ultrafast intraband relaxation and exciton multiplication in PbS quantum dots, *ACS Photonics* **1**, 285 (2014).
- [26] A. R. S. Kandada and C. Silva, Exciton polarons in two dimensional hybrid metal halide perovskites, *J. Phys. Chem. Lett.* **11**, 3173 (2020).
- [27] G. Y. Jia, Y. Liu, J. Y. Gong, D. Y. Lei, D. L. Wang, and Z. X. Huang, Excitonic quantum confinement modified optical conductivity of monolayer and few layered MoS₂, *J. Mater. Chem. C* **4**, 8822 (2016).
- [28] H. Khoirunnisa and M. A. Majidi, Exploring excitonic signal in optical conductivity of ZnO through first order electron-hole vertex correction, *J. Phys.: Conf. Ser.* **1011**, 012073 (2018).
- [29] R. W. Havener, Y. Liang, L. Brown, L. Yang, and J. Park, Van Hove singularities and excitonic effects in the optical conductivity of twisted bilayer graphene, *Nano Lett.* **14**, 3353 (2014).
- [30] H. Haug and S. W. Koch, Semiconductor laser theory with many-body effects, *Phys. Rev. A* **39**, 1887 (1989).
- [31] C. Ell, R. Blank, S. Benner, and H. Haug, Simplified calculations of the optical spectra of two and three dimensional laser excited semiconductors, *J. Opt. Soc. Am. B* **6**, 2006 (1989).
- [32] N. M. R. Peres, R. M. Ribeiro, and A. H. C. Neto, Excitonic Effects in the Optical Conductivity of Gated Graphene, *Phys. Rev. Lett.* **105**, 055501 (2010).
- [33] S. Yang, S. Tongay, Y. Li, Q. Yue, J. B. Xia, S. S. Li, J. Li, and S. H. Wei, Layer dependent electrical and optoelectronic responses of ReSe₂ nanosheet transistors, *Nanoscale* **6**, 7226 (2014).
- [34] R. S. Chen, C. C. Tang, W. C. Shen, and Y. S. Huang, Thickness dependent electrical conductivities and ohmic contacts in transition metal dichalcogenides multilayers, *Nanotechnology* **25**, 415706 (2014).

- [35] D. Qin, P. Yan, G. Ding, X. Ge, H. Song, and G. Gao, Monolayer PdSe₂: A promising two dimensional thermoelectric material, *Sci. Rep.* **8**, 2764 (2018).
- [36] Y. Ge, W. Wenhui, R. Yulu, and L. Yong, Large thermoelectric power factor of high mobility transition metal dichalcogenides with 1T phase, *Phys. Rev. Res.* **2**, 013134 (2020).
- [37] J. P. Ansermet and S. D. Brechet, Magnetic contribution to the Seebeck effect, *Entropy* **20**, 912 (2018).
- [38] U. I. Erkaboev, G. Gulyamov, J. I. Mirzaev, and R. G. Rakhimov, Modeling on the temperature dependence of the magnetic susceptibility and electrical conductivity oscillations in narrow gap semiconductors, *Int. J. Mod. Phys. B* **34**, 2050052 (2020).
- [39] Y. Jiang, Shula Chen, W. Zheng, B. Zheng, and A. Pan, Inter-layer exciton formation relaxation and transport in TMD van der Waals heterostructures, *Light: Sci. Appl.* **10**, 72 (2021).
- [40] V. Kattoor, K. Awasthi, E. Jokar, E. W. G. Diau, and N. Ohta, Enhanced dissociation of hot excitons with an applied electric field under low power photoexcitation in two dimensional perovskite quantum wells, *J. Phys. Chem. Lett.* **10**, 4752 (2019).
- [41] M. Van der Donck, M. Zarenia, and F. M. Peeters, Excitons triions and biexcitons in transition metal dichalcogenides: Magnetic field dependence, *Phys. Rev. B* **97**, 195408 (2018).
- [42] S. I. Nam, Electrical conductivity of quark matter at finite T under external magnetic field, *Phys. Rev. D* **86**, 033014 (2012).
- [43] A. Das, H. Mishra, and R. K. Mohapatra, Magneto Seebeck coefficient and Nernst coefficient of a hot and dense hadron gas, *Phys. Rev. D* **102**, 014030 (2020).
- [44] M. Tahir, P. Vasilopoulos, and F. M. Peeters, Magneto optical transport properties of monolayer phosphorene, *Phys. Rev. B* **92**, 045420 (2015).
- [45] C. C. Homes, M. Ali, and R. J. Cava, Optical properties of the perfectly compensated semimetal WTe₂, *Phys. Rev. B* **92**, 161109(R) (2015).
- [46] D. K. Efimkin and A. H. MacDonald, Exciton polarons in doped semiconductors in a strong magnetic field, *Phys. Rev. B* **97**, 235432 (2018).
- [47] S. Chaudhary, C. Knapp, and G. Refael, Anomalous exciton transport in response to a uniform in-plane electric field, *Phys. Rev. B* **103**, 165119 (2021).
- [48] A. Balocchi, Q. H. Duong, P. Renucci, B. Liu, C. Fontaine, T. Amand, D. Lagarde, and X. Marie, Full Electrical Control of the Electron Spin Relaxation in GaAs Quantum Wells, *Phys. Rev. Lett.* **107**, 136604 (2011).
- [49] E. Kasapoglu, H. Sari, M. Bursal, and I. Sokmen, Exciton absorption in quantum well wires under the electric field, *Physica E* **16**, 237 (2003).
- [50] E. M. Proupin and C. T. Giner, Electric field and exciton structure in CdSe nanocrystals, *Phys. Rev. B* **69**, 125336 (2004).
- [51] K. Cong, G. T. Noe II, and J. Kono, Excitons in magnetic fields, *Encycl. Mod. Optics II* **2**, 63 (2018).
- [52] N. Myoung, G. Ihm, and S. J. Lee, Transport in armchair graphene nanoribbons moduled by magnetic barriers, *Physica E* **42**, 2808 (2010).
- [53] S. Ghosh and M. Sharma, Electron optics with magnetic vector potential barriers in graphene, *J. Phys.: Condens. Matter* **21**, 292204 (2009).
- [54] C. Kenfack-Sadem, A. K. Teguimfouet, A. Kenfack-Jiotsa, and R. M. K. Tsiaze, Dynamics and decoherence of exciton polaron in monolayer transition metal dichalcogenides, *J. Electron. Mater.* **50**, 2911 (2021).
- [55] A. Thilagam and J. Singh, Excitonic polarons in quasi two dimensional structures, *Appl. Phys. A* **62**, 445 (1996).
- [56] V. K. Kozin, V. A. Shabashov, A. V. Kavokin, and I. A. Shelykh, Anomalous Exciton Hall Effect, *Phys. Rev. Lett.* **126**, 036801 (2021).
- [57] G. Pizzi, D. Volja, B. Kozinsky, M. Fornari, and N. Marzari, An updated version of Boltzmann: A code for the evaluation of thermoelectric and electronic transport properties with a maximally localized Wannier functions basis, *Comput. Phys. Commun.* **185**, 2311 (2014).
- [58] M. J. Tomczak, K. Haule, T. Miyake, A. Georges, and G. Kotliar, Thermopower of correlated semiconductors: Application to FeAs₂ and FeSb₂, *Phys. Rev. B* **82**, 085104 (2010).
- [59] S. Huang, H. J. Liu, D. D. Fan, P. H. Jiang, J. H. Liang, G. H. Cao, R. Z. Liang, and J. Shi, First principles study of the thermoelectric properties of the Zintl compound KSnSb, *J. Phys. Chem. C* **122**, 4217 (2018).
- [60] J. T. Devreese, *Frohlich Polarons: Lecture Course Including Detailed Theoretical Derivation* (Antwerp, Belgium, 2018).
- [61] M. Oliva-Leyva and C. Wang, Magneto optical conductivity of anisotropic two dimensional Dirac Weyl materials, *Ann. Phys.* **384**, 61 (2017).
- [62] C. Meier, S. Lüttjohann, M. Offer, H. Wiggers, and A. Lorke, Silicon nanoparticles: Excitonic fine structure and oscillator strength, *Adv. Solid State Phys.* **48**, 79 (2009).
- [63] D. Kozawa, R. Kumar, A. Carvalho, K. K. Amara, W. Zhao, S. Wang, M. Toh, R. M. Ribeiro, A. H. C. Neto, K. Matsuda, and G. Eda, Photocarrier relaxation pathway in two dimensional semiconducting transition metal dichalcogenides, *Nat. Commun.* **5**, 4543 (2014).
- [64] M. F. C. Fobasso, C. Kenfack-Sadem, E. Baloitcha, A. J. Fotue, and L. C. Fai, Lifetime and dynamics of polaron and bipolaron in graphene nanoribbon under laser, *Eur. Phys. J. Plus* **135**, 471 (2020).
- [65] Y. Xiao, Z. Q. Li, and Z. W. Wang, Polaron effect on the bandgap modulation in monolayer transition metal dichalcogenides, *J. Phys.: Condens. Matter* **29**, 485001 (2017).
- [66] A. Oukerroum, E. Feddi, J. B. Bailach, J. M. Pastor, F. Dujardin, and E. Assaid, On the anomalous Stark effect in a thin disc-shaped quantum dot, *J. Phys.: Condens. Matter* **22**, 375301 (2010).
- [67] M. Ghali, J. Kossut, E. Janik, F. Teppe, M. Vladimirova, and D. Scalbert, Spin precession in a model structure for spintronics, *AIP Conf. Proc.* **772**, 1383 (2005).
- [68] T. Yan, S. Yang, D. Li, and X. Cui, Long valley relaxation time of free carriers in monolayer WSe₂, *Phys. Rev. B* **95**, 241406(R) (2017).
- [69] H. Xu, J. Wei, H. Zhou, J. Feng, T. Xu, H. Du, C. He, Y. Huang, J. Zhang, Y. Liu, H. C. Wu, C. Guo, X. Wang, Y. Guang, H. Wei, Y. Peng, W. Jiang, G. Yu, and X. Han, High spin Hall conductivity in large area type II Dirac semimetal PtTe₂, *Adv. Mater.* **32**, 2000513 (2020).
- [70] A. Das, H. Mishra, and R. K. Mohapatra, Electrical conductivity and Hall conductivity of a hot and dense hadron gas in a magnetic field: A relaxation time approach, *Phys. Rev. D* **99**, 094031 (2019).
- [71] J. R. Djomou, S. C. Kenfack, A. J. Fotue, M. F. C. Fobasso, and L. C. Fai, Contribution of bulk and surface phonons to

- the properties of polaron in a $\text{Zn}_{1-x}\text{Cd}_x\text{Se}/\text{ZnSe}$ heterojunction confined in a triangular potential, *Phys. B: Condens. Matter* **548**, 58 (2018).
- [72] J. V. Nguepnang, A. K. Teguemfouet, C. S. Kenfack, and A. J. Kenfack, Polaron dynamic and decoherence in transition metal dichalcogenides under electric field, *Indian J. Phys.* **96**, 2001 (2022).
- [73] S. Kim, C. Lee, Y. S. Lim, and J. H. Shim, Investigation for thermoelectric properties of the MoS_2 monolayer-graphene heterostructure: Density functional theory calculations and electrical transport measurements, *ACS Omega* **6**, 278 (2021).
- [74] B. Skinner and L. Fu, Large nonsaturating thermopower in a quantizing magnetic field, *Sci. Adv.* **4**, eaat2621 (2018).
- [75] J. Hong, C. Lee, J. S. Park, and J. H. Shim, Control of valley degeneracy in MoS_2 by layer thickness and electric field and its effect on thermoelectric properties, *Phys. Rev. B* **93**, 035445 (2016).
- [76] M. Buscema, M. Barkelid, V. Zwiller, H. S. J. Van der Zant, G. A. Steele, and A. C. Gomez, Large and tunable photothermoelectric effect in single layer MoS_2 , *Nano Lett.* **13**, 358 (2013).
- [77] V. G. Kravets, V. V. Prorok, L. V. Poperenko, and I. A. Shaykevich, Ellipsometry and optical spectroscopy of low dimensional family TMDs, *Semiconductor Phys.-Quantum Electron. Optoelectron.* **20**, 284 (2017).
- [78] P. F. Li and Z. W. Wang, Optical absorption of Frohlich polaron in monolayer transition metal dichalcogenides, *J. Appl. Phys.* **123**, 204308 (2018).
- [79] M. Baira, M. Aljaghwan, B. Salem, N. A. Madhar, and B. Ihi, Investigation of GeSn/Ge quantum dots optical transitions for integrated optics on Si substrate, *Results Phys.* **12**, 1732 (2019).